Available online at www.sciencedirect.com

ScienceDirect

journal homepage: www.elsevier.com/locate/he

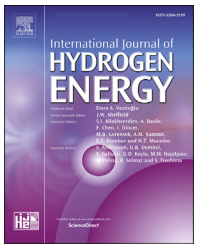

Tensile behaviour of 42CrMo4 steel submitted to annealed, normalized, and quench and tempering heat treatments with in-situ hydrogen charging

A. Imdad [a,*], V. Arniella [a], A. Zafra [b], J. Belzunce [a]

[a] Materials Science Department, University of Oviedo, Campus universitario, 33203 Gijón, Spain
[b] Imperial College London, UK

HIGHLIGHTS

- When hydrogen was introduced during the tensile test, a substantial decrease in notched strength was observed.
- Hydrogen embrittlement indexes increased as the steel hardness increases.
- Bainitic and ferrito-pearlitic microstructures were seen to be more susceptible to HE than quenched and tempered ones.

ARTICLE INFO

Article history:
Received 4 July 2023
Received in revised form
5 October 2023
Accepted 7 October 2023
Available online 20 October 2023

Keywords:
42CrMo4 steel
Heat treatments
Hydrogen embrittlement
In-situ hydrogen charging
Failure micromechanisms

ABSTRACT

42CrMo4 steel was submitted to annealing, normalizing, and quench and tempering heat treatments to produce steel microstructures with different hardness levels. Afterwards, tensile tests using notched specimens were conducted in air and in two different hydrogenated conditions by means of *in-situ* electrochemical hydrogen charging tests. Two different electrolytes and density currents were employed to produce low and high hydrogenated conditions. The influence of microstructure and hardness on hydrogen embrittlement was determined and scanning electron microscopy (SEM) analysis was used to identify the respective operative failure micromechanisms. A significant loss in notched strength was observed when hydrogen was introduced during the tensile tests on all tested microstructures, giving rise to changes in the predominant operative failure micromechanism. Embrittlement indexes increase as the electrochemical conditions applied introduce higher hydrogen concentrations and as the steel hardness increases. The notched tensile strength measured with in-situ hydrogen charging in the normalized and annealed grades is lower than that of quenched and tempered steels for the same hardness.

1. Introduction

Global energy demand is expected to rise by over 45% by 2030 driven by the expansion of the economics of underdeveloped nations [1]. This will cause an acceleration of global warming and air contamination. Therefore, the time has come to prioritize clean and renewable energy sources over fossil fuels. The demand for hydrogen will soar in the near future, as it is a clean, safe, and cost-effective energy vector [2]. Many

* *Corresponding author.*
E-mail address: uo256361@uniovi.es (A. Imdad).
https://doi.org/10.1016/j.ijhydene.2023.10.082

different metallic components must be constructed to manage hydrogen pressure. These include pressure vessels and other containers, pipelines and valves, which will be directly exposed to high-pressure hydrogen gas environments. Thus, there is a widespread interest in the development of economic medium and high-strength steels able to store and transport hydrogen safely [3].

The impact of hydrogen on the tensile properties of medium and high strength steels in contact with high pressure hydrogen gas has been widely researched [4,5]. It is now well known that this class of steels is prone to hydrogen embrittlement (HE), which produces a notorious degradation of their most important mechanical properties (tensile strength, elongation, fracture toughness, and fatigue crack propagation rate) [6–9]. Atomic hydrogen enters and diffuse through the steel lattice under the influence of stress and concentration gradients [10–12]. Hydrogen atoms become trapped in different lattice defects, called hydrogen traps [13,14], where different damage processes can take place, modifying the operative failure micromechanisms [15,16]. In the case of steels, hydrogen-enhanced decohesion (HEDE) along certain internal interfaces, hydrogen-enhanced localized plasticity (HELP) and adsorption induced dislocation emission (AIDE) are the most cited hydrogen-assisted micromechanisms [17]. In reality, it is now widely recognized that the HE phenomenon is controlled by a combination of a determined amount of hydrogen that has accumulated in particular areas of the steel microstructure and critical stress/strain levels [18,19]. Depending on the strength level of steel and on the concentration of internal hydrogen, hydrogen typically induces brittle fractures, with fracture surfaces characterized by cleavage or intergranular fracture, although ductile microvoids coalescence fractures were also sometimes observed with the most ductile structural steel grades. Among the many research works on the detrimental effects of hydrogen on the tensile properties of structural steels published over recent decades is the CHMC1-2014 document by the Canadian Standards Association (CSA). This work assesses the compatibility of materials with hydrogen [20]. Simple screening slow-strain rate tensile tests performed with smooth or notched specimens under specific hydrogen pressure were proposed and hydrogen embrittlement indices (HEI) related to reduction of area or to the notch tensile strength were recommended. This standard categorizes materials satisfying the condition HEI <10% as suitable and HEI >50% as non-suitable for hydrogen services under the provided pressure. All other materials are considered hydrogen embrittled and must undergo fracture toughness and fatigue testing in such gaseous hydrogen condition for compatibility assessment.

The effect of hydrogen on the tensile behaviour of medium-high strength steels depends on many factors. These include the dimensions and geometry of the specimens, the stress concentration factor (in the case of notched specimens), the steel microstructure (chemical composition and heat treatment) and the strength of the steel. In addition, various testing variables must be considered, including the applied displacement or strain rate, the hydrogenation medium (hydrogen pressure with hydrogen gas or electrolyte and current density in the case of hydrogen electrochemical charged from aqueous solutions) and the temperature of the test [21,22].

The influence of microstructure on hydrogen embrittlement susceptibility was examined by Naninga et al. [23] comparing notched tensile specimens of steel cathodically charged with hydrogen at a fixed potential. While the values of notch failure stress of the specimens tested in air increase approximately linearly with the increase in hardness, when the specimens were tested with hydrogen, the resultant notch failure stress decreased with hardness. The strength of the steel is the dominant factor in hydrogen embrittlement with microstructure playing a secondary role. The susceptibility of different microstructures of structural steels (ferrite, pearlite, ferrite + pearlite, bainite and martensite) was studied by Michler et al. [24] through reduction of area measurements in tensile tests performed in air and in 10 MPa hydrogen gas. A clear correlation was obtained between hydrogen embrittlement index and the steel microstructure. However, grain size was not found to have a significant influence. Ogawa et al. [25] used slow strain-rate tensile tests in 95 MPa hydrogen gas on ferrite-pearlite steels with varying carbon contents to show that hydrogen has only a minor impact on yield and ultimate tensile strength. However, it led to severe decreases in elongation and in reduction of area, the magnitude of this degradation being more pronounced with increased carbon content (higher steel strength).

The effect of hydrogen on notched tensile properties can be important. For example, both ductility and strength can be reduced significantly [26]. Wang et al. [27] demonstrated hydrogen embrittlement increases with the stress concentrator factor, k_t (higher notch length or lower notch tip radius) in notched tensile tests performed with the same initial hydrogen concentration. In these tests, hydrogen accumulates just ahead of the notch tip, where local hydrostatic stress attains maximum values, giving rise to high local hydrogen concentrations. Lower stress is then required to break the specimen. Since the level of hydrostatic stress that develops in the notch tip region is proportional to the yield strength of the steel, hydrogen embrittlement always increases with yield strength [23,25]. Tests performed under very low displacement rates exacerbate the adverse impact of hydrogen, as hydrogen atoms have more time to diffuse through the steel microstructure, eventually leading to higher hydrogen concentrations in the process zone [28–30]. On the other hand, Barthelemy et al. [31] reported a 50% reduction in the fracture toughness of a plain carbon steel tested in gaseous hydrogen at 6.9 MPa and, similarly, Ogawa et al. [32] performed fracture toughness tests in a low carbon non-alloyed steel in air and in hydrogen gas under pressures of 0.7 and 115 MPa, noticing a significant degradation on the fracture toughness manifested in the load-displacement curves and also in the J-toughness crack growth curves.

The purpose of this research is to examine the mechanical behaviour of notched tensile specimens of 42CrMo4 steel subjected to different heat treatments, carefully designed to provide different microstructures. Electrochemical hydrogen charging was applied during the tensile tests (in-situ hydrogen charging or external hydrogen condition) and two different hydrogenation conditions were also applied. The operative

failure micromechanisms were identified and correlated with steel microstructures and hardness or strength.

2. Materials and experimental procedure

2.1. Material and heat treatment

A commercial 42CrMo4 steel (AISI 4140) was employed in this work. Table 1 displays its chemical composition. The steel was delivered as a hot rolled plate with a thickness of 12 mm. It is a medium carbon steel mainly alloyed with chromium and molybdenum, which is considered to be an excellent choice to be used in services under high-pressure hydrogen [33]. The steel was submitted to normalizing, annealing and quenching and tempering treatments. Table 2 shows the different heat treatments applied. An austenitization temperature of 845 °C was employed but, in the case of normalized (air cooled) and annealed (furnace cooled) grades, a temperature of 1050 °C was also used to study the effect of prior austenite grain size in hydrogen embrittlement. After quenching in water from 845 °C, two different tempering conditions were also employed for the quenched and tempered grades (600 °C for 2 h and 725 °C for 4 h) to obtain hardness values similar to those of the normalized and annealed grades. Vickers hardness (HV30) was determined under a load of 30 kg. Tensile tests were also performed in air on standard cylindrical specimens with a diameter of 5 mm and a calibrated length of 28 mm.

Table 1 – Chemical composition of 42CrMo4 steel (weight %).

Steel	%C	%Cr	%Mo	%Mn	%P	%S
42CrMo4	0.42	0.98	0.22	0.62	0.008	0.002

Table 2 – Heat treatments: FC = Furnace cooled, AC = Air cooled, QT = Quenched and tempered.

Steel grade		Heat treatment
845-FC	Annealed	845 °C/40min + FC
1050-FC		1050 °C/40min + FC
845-AC	Normalized	845 °C/40min + AC
1050-AC		1050 °C/40min + AC
QT-600	Quench and tempered	845 °C/40min + 600 °C/2h
QT-725		845 °C/40min + 725 °C/4h

2.2. Tensile tests

Tensile tests were carried out according to ISO 6892–1:2017 standard [34], at room temperature on an Instron 5582 tensile testing machine using circumferentially notched round-bar specimens, whose dimensions and geometry are illustrated in Fig. 1(a).

Tensile tests were conducted in three different testing conditions. The first test was always conducted in a hydrogen-free environment (in air) at a standard displacement rate of 0.4 mm/min. The other two tests were carried out with in-situ electrochemical hydrogen charging using two different conditions: the first in an acidic aqueous solution 1 M H_2SO_4 with a current density of 1 mA/cm^2 (low hydrogen); the second in the same acidic solution with an addition of 0.25 g/l of As_2O_3 with a current density of 0.5 mA/cm^2 (high hydrogen). As_2O_3 addition prevents hydrogen atoms from recombining (H + H → H_2), more hydrogen accumulates on the surface of the metal, and a larger hydrogen concentration enters the sample

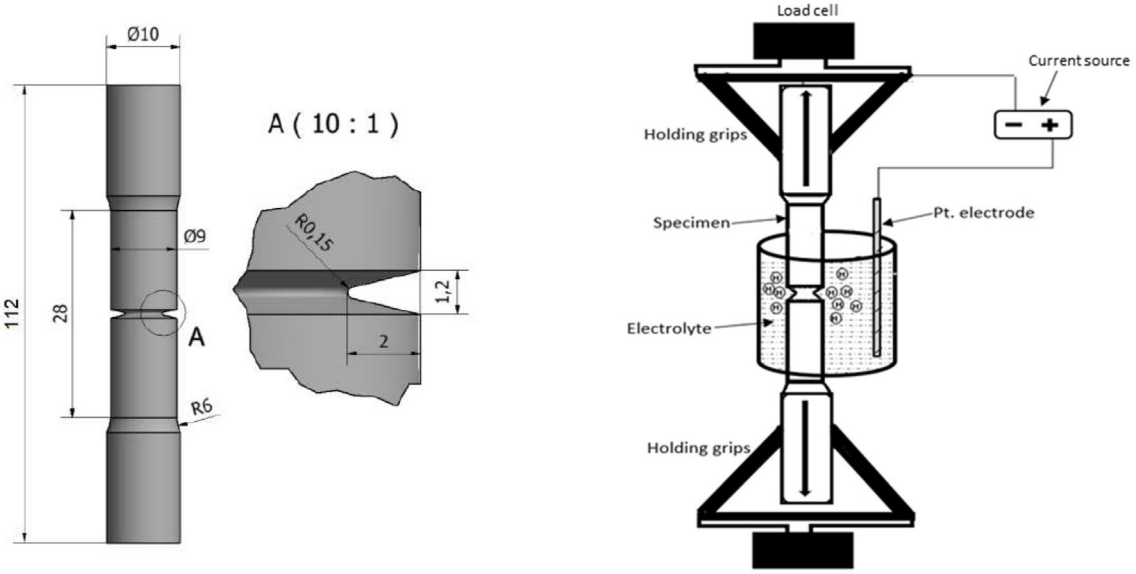

Fig. 1 – (a) Geometry and dimensions (mm) of notched tensile specimens and (b) scheme of the in-situ hydrogen charging tensile test performed on notched specimens.

[35–37]. In these low and high hydrogen charging conditions, hydrogen contents of 0.5 and 0.95 wppm, respectively, were measured in the same steel (quenched and tempered at 700 °C for 2 h, 223 HV) [38]. The former corresponds to a typical service under high pressure hydrogen (Yamabe et al. [39] measured hydrogen contents around 0.5 ppm using gaseous charging under an hydrogen pressure of 100 MPa) and the latter introduces approximately twice this hydrogen content into the steel.

In all these in-situ hydrogen-charged tests, a low displacement rate, 0.01 mm/min, was used to allow sufficient time for hydrogen diffusion and accumulation, thus facilitating hydrogen embrittlement. Fig. 1(b) shows a scheme of the in-situ electrochemical hydrogen charged test employed in this work. The stress applied was continuously monitored against the elongation of the specimens, and the ultimate notched strength at failure, σ_{uN}, was determined by dividing the highest recorded tensile load by the initial cross-sectional area measured in the notch region. The degree of hydrogen embrittlement was quantified using the hydrogen embrittlement index (HEI), provided by Equation (1): HEI goes from 0% (no embrittlement, $X = X_H$) to 100% (highest possible hydrogen embrittlement, when $X_H = 0$).

$$HEI\,\% = \frac{X - X_H}{X} \cdot 100 \tag{1}$$

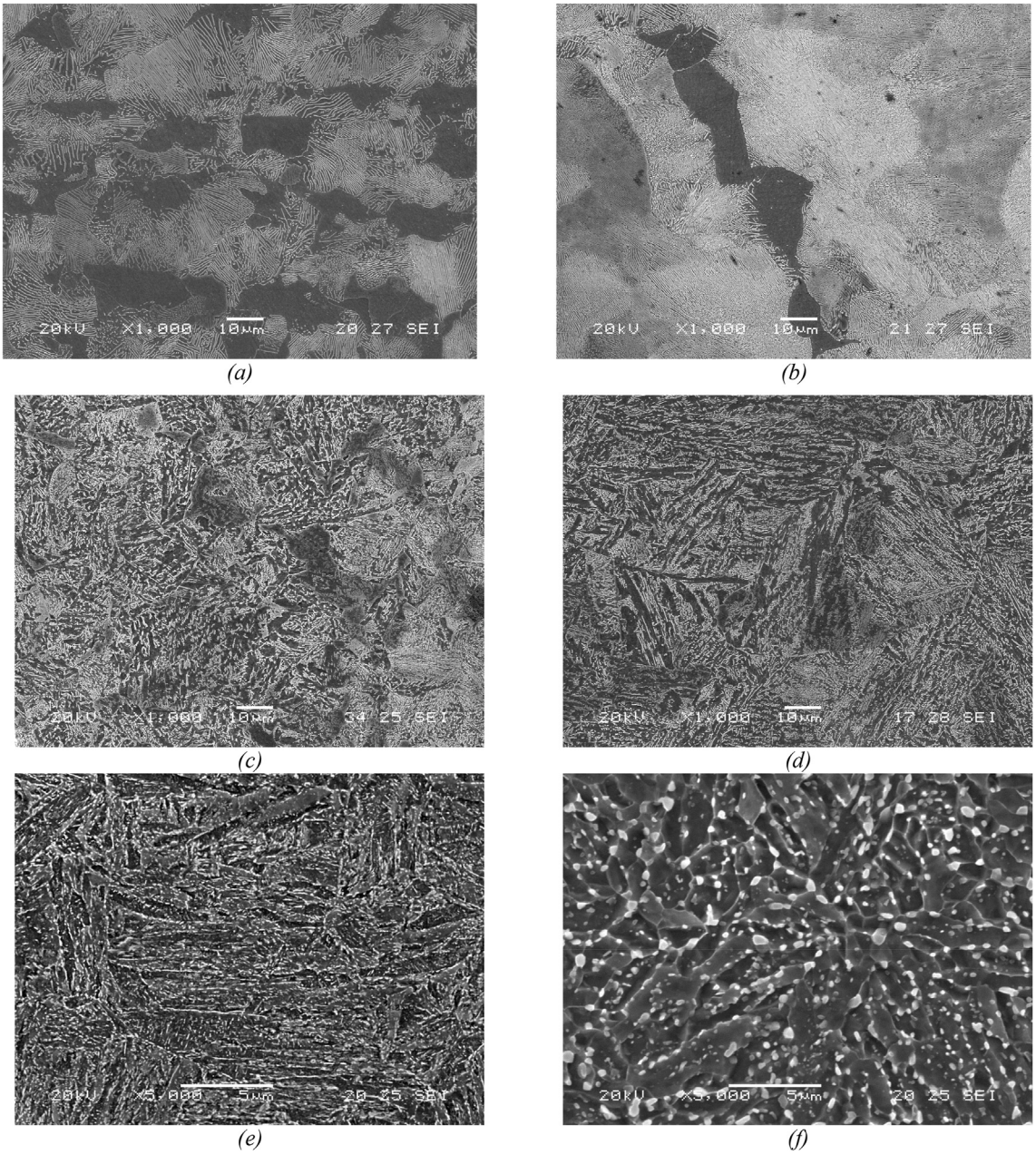

Fig. 2 – Steel microstructures, a) annealed at 845 °C, b) annealed at 1050 °C, c) normalized at 845 °C, d) normalized at 1050 °C, e) quenched and tempered at 600 °C, f) quenched and tempered at 725 °C.

Table 3 – Hardness, tensile properties and microstructures of 42CrMo4 grades.

Steel grades	Microstructures	Hardness (HV30)	Yield strength (MPa)	Ultimate tensile strength (MPa)	Elongation (e) %
845-FC	Ferrite-pearlite (banded)	183 ± 6	336	664	20.1
1050-FC	Ferrite-pearlite	210 ± 3	344	740	13.3
845-AC	Mainly bainite	301 ± 3	677	1008	13.0
1050-AC	Mainly bainite	285 ± 8	708	961	13.1
QT-600	Tempered martensite	307 ± 4	910	1002	15.0
QT-725	Tempered martensite	206 ± 3	526	607	22.0

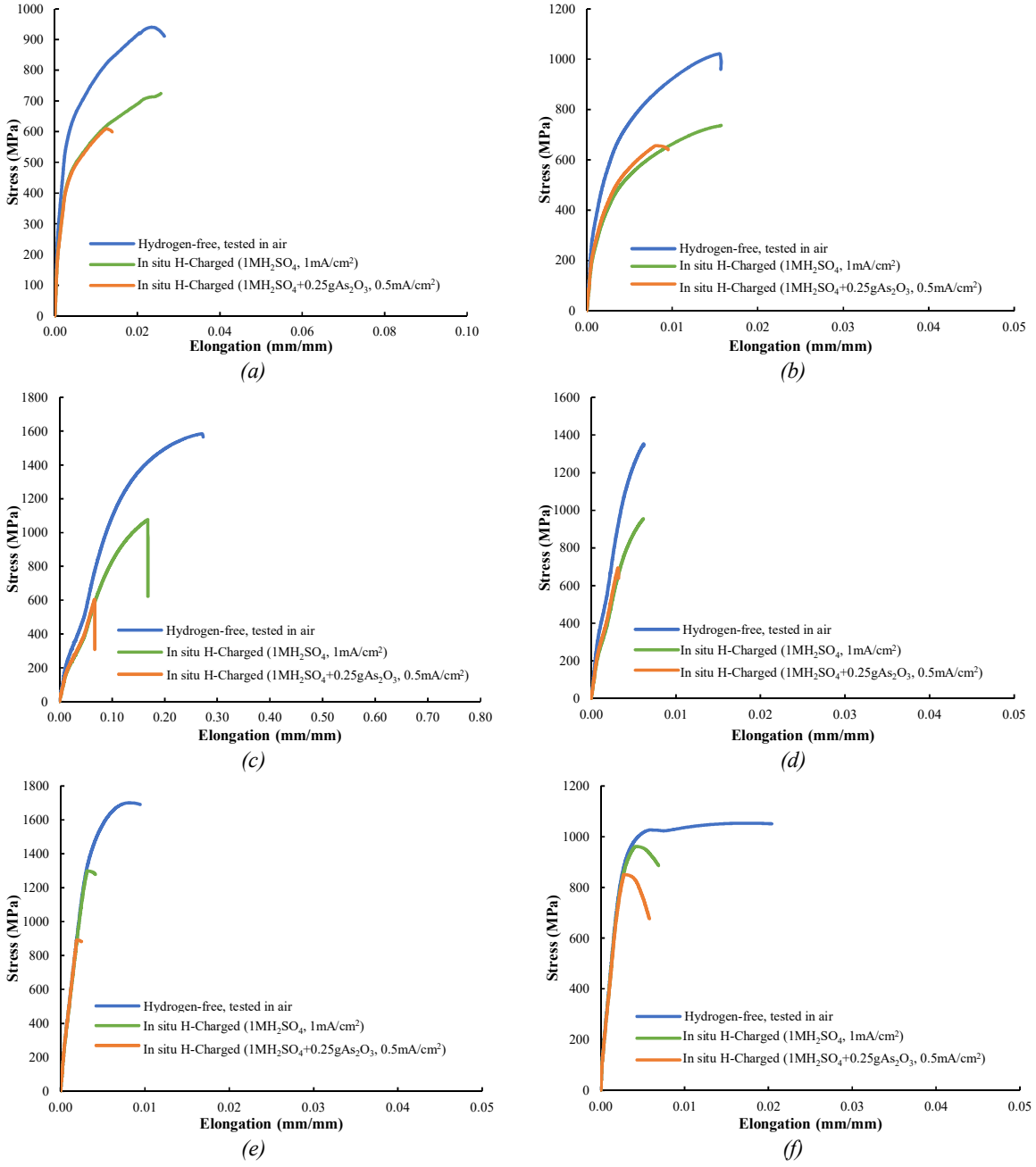

Fig. 3 – Stress-strain curves of notched tensile tests performed on a) 845-FC, b) 1050-FC, (c) 845-AC, (d) 1050-AC, (e) QT-600, (f) QT-725.

where X and X_H are the measured steel property evaluated without and with hydrogen respectively (in this case the notch tensile strength, σ_{uN}).

3. Results and discussion

3.1. Microstructures and hardness

Ferrite-pearlite microstructures were produced after the annealing treatments (Fig. 2 a, b). A banded ferrite-pearlite microstructure was present in the grade that was annealed at the lowest temperature (845 °C), but banding disappeared when annealing at 1050 °C. The slightly lower hardness measured in the steel austenitized at 845 °C (845-FC) is justified by the presence of a higher fraction of ferrite (see hardness values in Table 3). Fig. 2 c) and d) presents the microstructures produced after the two normalizing treatments. They are mostly bainite, slightly more refined and with a greater hardness when the lowest austenitizing temperature was applied (845-AC). Finally, the quenched and tempered grades consist of tempered martensite microstructures (Fig. 2 e, f) with hardness similar to the other grades: QT-600 and normalized samples have comparable hardness (around 300 HV) and the same occurs with QT-725 and the annealed grades (around 200 HV). After tempering at 600 °C, elongated carbides precipitated along block, packet and lath martensite boundaries, although structural acicularity is still present. Tempering at 725 °C produced a fully tempered, relaxed, and recrystallized microstructure with well distributed globular carbides. The hardness, yield strength and tensile strength of all these 42CrMo4 grades are shown in Table 3.

3.2. Notched tensile tests

Fig. 3 shows the stress-strain curves obtained with notched tensile specimens in the different conditions tested with all the grades studied. In all cases, the entrance of hydrogen clearly decreases the notched tensile strength and greatly decreases the elongation at failure. These effects are greater with the higher hydrogen condition (solution with arsenic oxide). It is also worth noting that failure in presence of hydrogen took place after minimum plastic deformation in the three grades with the greatest hardness (both normalized grades and QT-600).

Table 4 includes the tensile test results obtained in all notched tensile tests, including the applied displacement rate, duration of each test, and the corresponding embrittlement index related to the notch strength. In general, in both hydrogenated conditions, as hardness and strength increase so do the corresponding embrittlement index. It is important to note that HEI was consistently higher in the solution containing arsenic oxide (high hydrogen), as more hydrogen enters the steel microstructure in this situation.

All tests performed in air, showed an initiation failure region next to the tip of the notch where the main failure micromechanism is ductile: dimples, coalescence of microcavities, MVC. However, this changed when samples were tested with simultaneous entrance of hydrogen. In all the tests conducted in presence of hydrogen (in both hydrogenated conditions), quasi-cleavage (QC) was the only failure initiation micromechanism. Some examples of such failures are presented in Fig. 4. Quasi-cleavage operative failure micromechanism with always low plasticity was predominant in the furnace cooled steel grade austenitized at higher temperature. While in the case of the air-cooled samples, the one austenitized at the highest temperature has much larger cleavage facets due to its larger prior austenite grain size. Cleavage facets have a smaller size and many more plasticity features in the two quenched and tempered grades. No vestige of MCV or intergranular fracture was observed in any of these samples.

4. Discussion

In this paper hydrogen embrittlement has been studied using notched tensile specimens with in-situ hydrogen charging.

Table 4 – Tensile tests results of notched specimens of 42CrMo4 grades.

Steel grade	Test conditions	Disp. rate (mm/min)	Time (min)	σ_{uN} (MPa)	HEI (%)
845-FC (183 HV)	Air	0.4	9	940	–
	Low H.	0.01	223	758	19
	High H.	0.01	166	610	35
1050-FC (210 HV)	Air	0.4	7	1021	–
	Low H.	0.01	221	763	25
	High H.	0.01	157	656	35
845-AC (301 HV)	Air	0.4	9	1585	–
	Low H.	0.01	154	1077	32
	High H.	0.01	114	605	62
1050-AC (285 HV)	Air	0.4	7	1348	–
	Low H.	0.01	271	953	29
	High H.	0.01	174	694	48
QT-600 (307 HV)	Air	0.4	7	1701	–
	Low H	0.01	331	1299	23
	High H	0.01	326	891	48
QT-725 (206 HV)	Air	0.4	8	1053	–
	Low H	0.01	278	961	9
	High H	0.01	212	851	19

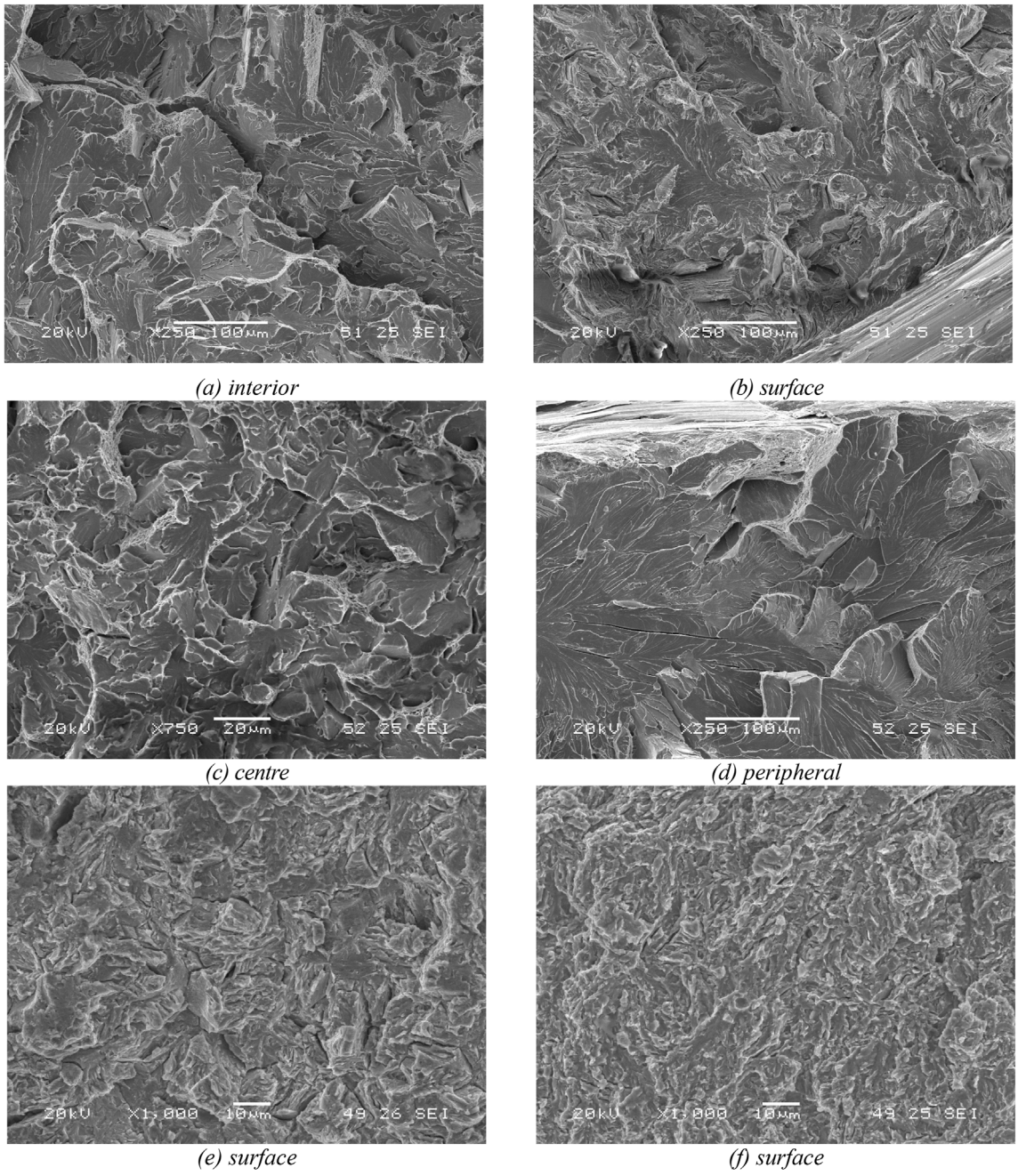

Fig. 4 – Failed surfaces of specimens tested in the solution with arsenic oxide (high hydrogen), (a) 845-FC, (b) 1050-FC, (c) 845- AC, (d) 1050-AC, (e) QT-600, (f) QT-725.

This condition is interesting because the effects of hydrogen are always more evident in presence of stress concentrators, as hydrogen enters from the hydrogenated medium into a plastically strained zone, diffuses and accumulates in the region ahead of the notch submitted to high hydrostatic stresses, where different decohesion phenomena such as intergranular cracking (HEDE mechanism) could take place [40].

The notched tensile strength of all the microstructures measured in air and in both hydrogenated conditions is plotted against the hardness of the steel in Fig. 5. The blue line shows the linear trend between the steel hardness and the notched tensile strength in tests performed in air. The slope of the line obtained with the annealed and normalized grades with in-situ hydrogen charging decreases as hydrogen content in the samples increases. Fig. 5 also shows that in these hydrogenated conditions, quenched and tempered grades (represented with green and orange triangles) always display a better behaviour than annealed and normalized grades.

The effect of the steel microstructure on the notched tensile strength measured in air and in tests performed with hydrogen charging is better understood by directly comparing the results obtained with different microstructures with similar hardness. Tempered martensite and

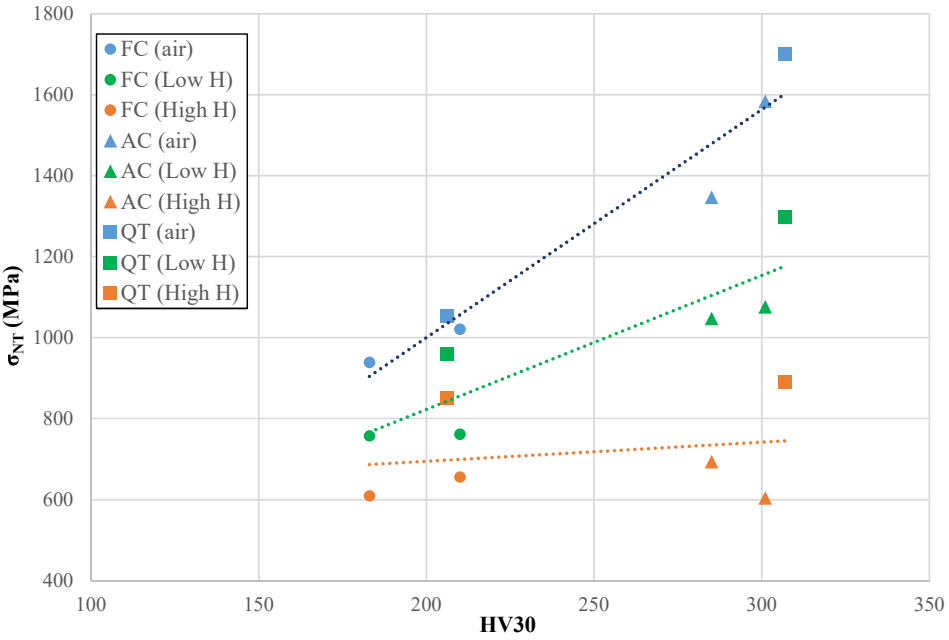

Fig. 5 – Notched tensile strength versus steel hardness. Air cooled, furnace cooled and quenched and tempered grades tested in air (blue symbols) and in low and high hydrogen conditions (green and orange symbols, respectively). (For interpretation of the references to colour in this figure legend, the reader is referred to the Web version of this article.)

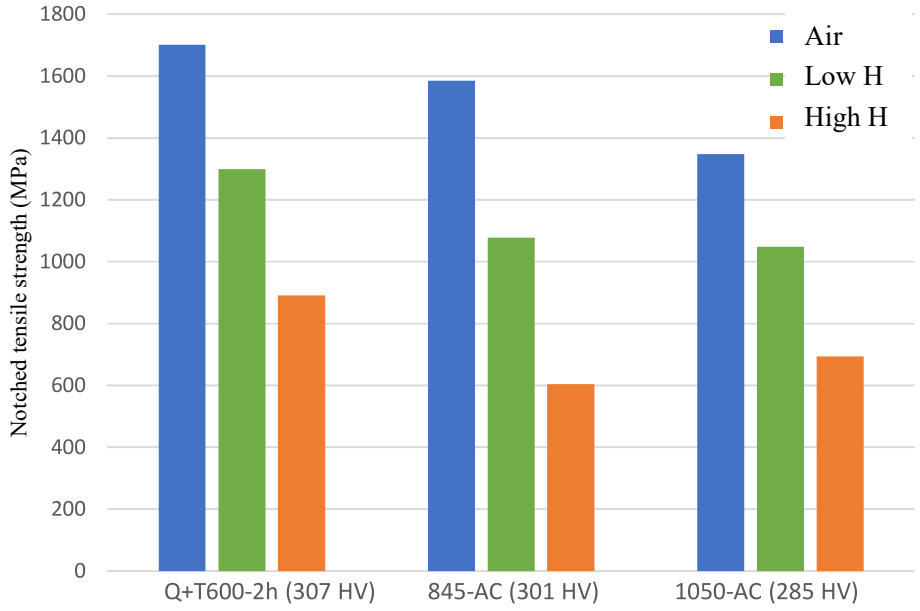

Fig. 6 – Notched tensile strength of tempered martensite (QT-600) and bainite microstructures (845-AC and 1050-AC). Tested in air (blue), in low hydrogen (green) and high hydrogen (orange) conditions. (For interpretation of the references to colour in this figure legend, the reader is referred to the Web version of this article.)

bainitic microstructures were compared using the results obtained with QT-600, 845-AC and 1050-AC grades, as these grades have similar hardnesses, 307, 301 and 285 HV respectively. Fig. 6 shows the results of the notched tensile strength obtained in these tests. Bainitic microstructures have significantly lower notched tensile strength in all tested conditions (air, low and high hydrogenated media) than tempered martensite microstructures.

Tempered martensite and ferrito-pearlitic microstructures were compared using the results obtained with QT-725, 845-FC and 1050-FC grades, as these grades had similar hardnesses, 206, 183 and 210 HV respectively.

Fig. 7 shows the results of the notched tensile strength obtained in these tests. Ferrito-pearlitic microstructures also have significantly lower notched tensile strength on all the

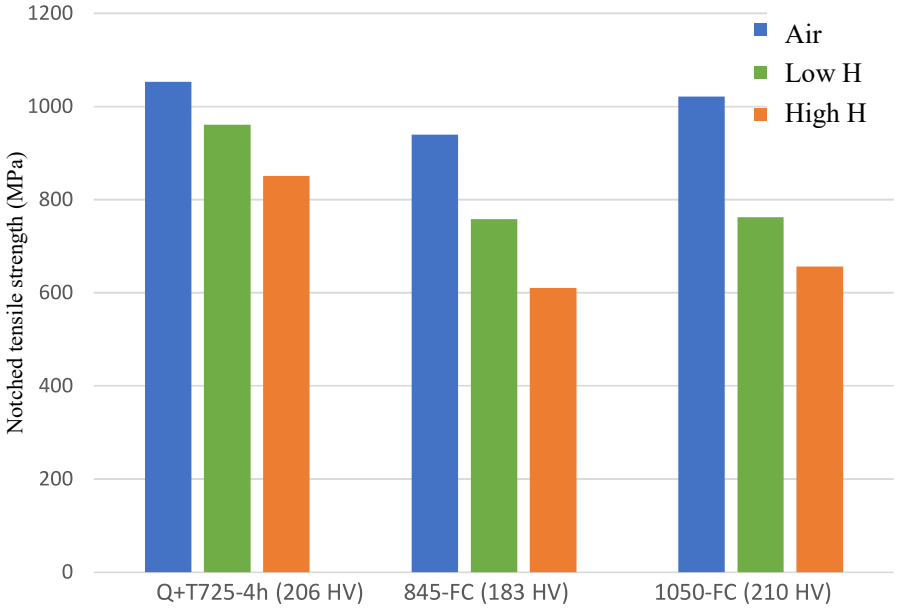

Fig. 7 – Notched tensile strength of tempered martensite (QT 725-4h) and ferrito-pearlitic microstructures (845FC and 1050FC). Tests in air (blue), in low hydrogen (orange) and high hydrogen (green) conditions. (For interpretation of the references to colour in this figure legend, the reader is referred to the Web version of this article.)

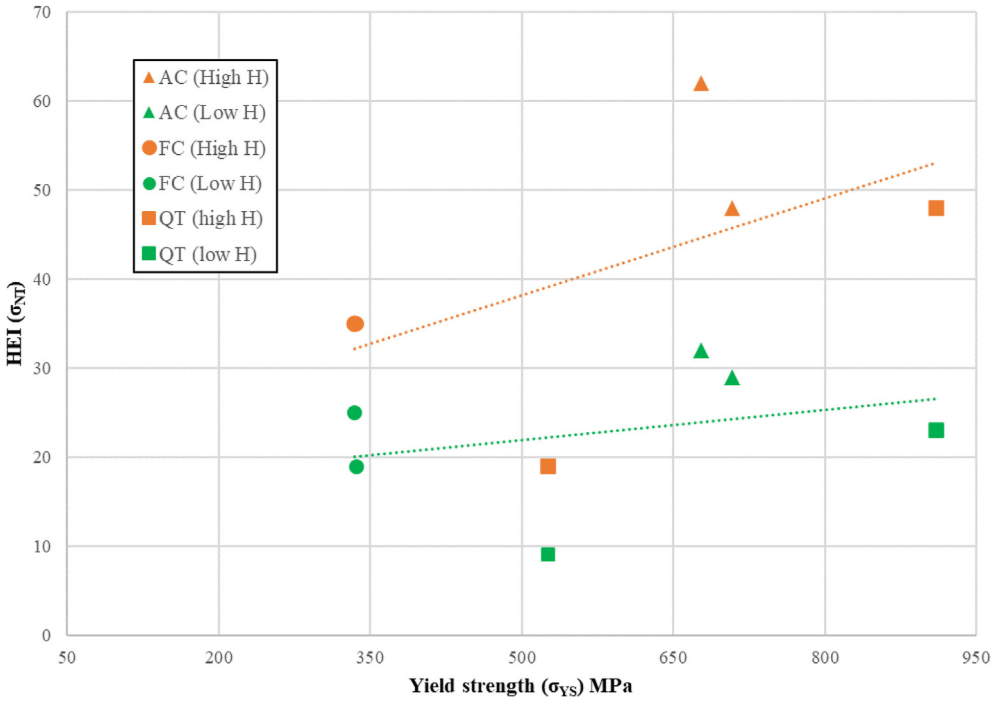

Fig. 8 – HEI related to notched tensile strength versus yield strength (σ_{ys}) for the AC, FC and Q + T grades tested in low (green symbols) and high (orange symbols) hydrogenated conditions. (For interpretation of the references to colour in this figure legend, the reader is referred to the Web version of this article.)

conditions tested (air, low and high hydrogenated media) than quenched and tempered ones.

Since yield strength is the property typically used in the design of structural components and to assess hydrogen embrittlement, Fig. 8 represents the hydrogen embrittlement indexes related to the notch tensile strength obtained in low and high hydrogenated conditions with all the steel grades studied against the steel yield strength. Hydrogen embrittlement indexes increase linearly with the yield strength of the steels in low and high hydrogenated media. Embrittlement indexes near or above 50% (steels non suitable for hydrogen service) were measured in both normalized grades and the

QT-600 steel, all with hardness of approximately 300 HV, when tested in the high hydrogenated condition. Only the quenched and tempered steel with the lowest yield strength and hardness, with a hydrogen embrittlement index below 10% when tested in the low hydrogenated condition is fully compatible with hydrogen. Finally, in general, lower hydrogen embrittlement indexes were obtained when the low austenitization temperature (845 °C) was used in the annealed and normalized grades. This effect is particularly clear in the case of the air-cooled samples. The sample austenitized at the highest temperature, with a larger prior austenite grain size, has lower hardness but a significantly larger HEI in both hydrogenated media. Much larger cleavage facets were also found on its failure surface (Fig. 4a and b).

5. Conclusions

A significant loss in notched strength was observed when hydrogen was introduced in the course of the in-situ electrochemically hydrogen charged notched tensile tests performed on all tested 42CrMo4 steel microstructures. Hydrogen embrittlement indexes increase as the applied electrochemical conditions introduce higher hydrogen levels and as the steel hardness increases.

Steels with hardness near or above 300 HV, with bainitic or tempered martensite microstructures proved to be not suitable for hydrogen service when tested in the high hydrogenated condition and only the Q + T grade with the lowest hardness, tempered at 725 °C for 4 h, can be considered fully compatible with hydrogen (HEI <10%) in the low hydrogenated condition.

The main failure micromechanism in all the notched tensile tests performed in air was ductile (coalescence of microcavities, MVC), but changed to quasi-cleavage (QC) when samples were tested with simultaneous entrance of hydrogen. Lower notched tensile strength with in-situ hydrogen charging was measured in the normalized and annealed grades than with the quenched and tempered grades with the same hardness.

Bainitic and ferrito-pearlitic microstructures are more susceptible to hydrogen embrittlement than quenched and tempered ones.

Finally, in general, lower hydrogen embrittlement indexes were obtained when the low austenitization temperature (845 °C) was used in the annealed and normalized grades.

Declaration of competing interest

The authors declare that they have no known competing financial interests or personal relationships that could have appeared to influence the work reported in this paper.

Acknowledgements

A. Zafra would like to thank the Spanish Ministry of Universities for the Margarita Salas Postdocotral Fellowships [reference MU-21-UP2021- 030] funded through the Next Generation EU programme. V. Arniella would also like to thank the Spanish Ministry of Science, Innovation and Universities for the financial support received through FPI grant PRE2019-088533. The authors would also like to acknowledge the technical support provided by the Scientific and Technical Service of the University of Oviedo for the use of the SEM JEOLJSM5600 scanning electron microscope.

REFERENCES

[1] WHO. Fact sheet: ambient (outdoor) air pollution. 2021.
[2] Barbier F, Basile A, Nejat Veziroglu T. Compendium of hydrogen energy. Vol. 3, 1st edition in Woodhead Publishing Series in Energy 2016.
[3] The future of hydrogen. Report prepared by the IEA for the G20, Japan. 2019.
[4] Briottet L, Batisse R, de Dinechin G, Langlois P, Thiers L. Recommendations on X80 steel for the design of hydrogen gas transmission pipelines. Int J Hydrogen Energy 2012;37(11):9423–30.
[5] Wang M, Akiyama E, Tsuzaki K. Effect of hydrogen on the fracture behavior of high strength steel during slow strain rate test. Corrosion Sci 2007;49(11):4081–97.
[6] Takagi S, Toji Y, Yoshino M, Hasegawa K. Hydrogen embrittlement resistance evaluation of ultra-high strength steel sheets for automobiles. ISIJ Int 2012;52:316–22. https://doi.org/10.2355/isijinternational.52.316.
[7] Zafra A, Peral LB, Belzunce J, Rodríguez C. Effects of hydrogen on the fracture toughness of 42CrMo4 steel quenched and tempered at different temperatures. Int J Pres Ves Pip 2019;171:34–50.
[8] Murakami Y, Kanezaki T, Sofronis P. Hydrogen embrittlement of high strength steels: determination of the threshold stress intensity for small cracks nucleating at nonmetallic inclusions. Eng Fract Mech 2012;97:227–43. https://doi.org/10.1016/j.engfracmech.2012.10.028.
[9] Colombo C, Fumagalli G, Bolzoni F, Gobbi G, Vergani L. Fatigue behavior of hydrogen pre-charged low alloy Cr-Mo steel. Int J Fatig 2015;83:2–9. https://doi.org/10.1016/j.ijfatigue.2015.06.002.
[10] Dadfarnia M, Sofronis P, Neeraj T. Hydrogen interaction with multiple traps: can it be used to mitigate embrittlement. Int J Hydrogen Energy 2011;36:10141–8. https://doi.org/10.1016/j.ijhydene.2011.05.027.
[11] Oriani RA. The diffusion and trapping of hydrogen in steel. Acta Metall 1970;18:147–57. https://doi.org/10.1016/0001-6160(70)90078-7.
[12] Wang Y, Wu X, Zhou Z, Li X. Numerical analysis of hydrogen transport into a steel after shot peening. Results Phys 2018;11:5–16. https://doi.org/10.1016/j.rinp.2018.08.030.
[13] McNabb A, Foster PK. A new analysis of the diffusion of hydrogen in iron and ferritic steels. Trans Metall Soc AIME 1963;227:618–27.
[14] Lee JY, Lee JL. A trapping theory of hydrogen in pure iron. Philos Mag A Phys Condens Matter Struct Defects Mech Prop 1987;56:293–309. https://doi.org/10.1080/01418618708214387.
[15] Robertson IM, Sofronis P, Nagao A, Martin ML, Wang S, Gross DW, Nygren KE. Hydrogen embrittlement understood. Metall Mater Trans B Process Metall Mater Process Sci 2015;46:1085–103. https://doi.org/10.1007/s11663-015-0325-y.
[16] Michler T, San Marchi C, Naumann J, Weber S, Martin M. Hydrogen environment embrittlement of stable austenitic

steels. Int J Hydrogen Energy 2012;37:16231–46. https://doi.org/10.1016/j.ijhydene.2012.08.071.
[17] Lynch SP. Hydrogen embrittlement (HE) phenomena and mechanisms, Stress Corros. Crack Theory Pract 2011:90–130. https://doi.org/10.1533/9780857093769.1.90.
[18] Miresmaeili R, Liu L, Kanayama H. A possible explanation for the contradictory results of hydrogen effects on macroscopic deformation. Int J Pres Ves Pip 2012;99–100:34–43. https://doi.org/10.1016/j.ijpvp.2012.08.001.
[19] Li X, Gong B, Deng C, Li Y. Effect of pre-strain on microstructure and hydrogen embrittlement of K-TIG welded austenitic stainless steel. Corrosion Sci 2019;149:1–17. https://doi.org/10.1016/j.corsci.2018.12.018.
[20] ANSI/CSA. CHMC 1-2014, Test method for evaluating material compatibility in compresses hydrogen applications –phase I-, Metals. Mississauga, ON. Canadian Standards Association; 2014.
[21] Wang M, Akiyama E, Tsuzaki K. Effect of hydrogen on the fracture behavior of high strength steel during slow strain rate test. Corrosion Sci 2007;49:4081–97. https://doi.org/10.1016/j.corsci.2007.03.038.
[22] Zafra A, Harris Z, Sun C, Martínez-Pañeda E. Comparison of hydrogen diffusivities measured by electrochemical permeation and temperature-programmed desorption in cold-rolled pure iron. J Nat Gas Sci Eng 2022;98:104365.
[23] Naninga N, Grochowsi J, Heldt L, Rundman K. Role of microstructure, composition and hardness in resisting hydrogen embrittlement of fastener grade steels. Corrosion Sci 2010;52:1237–46. https://doi.org/10.1016/j.corsci.2009.12.020.
[24] Zafra A, Peral LB, Belzunce J, Rodríguez C. Effect of hydrogen on the tensile properties of 42CrMo4 steel quenched and tempered at different temperatures. Int J Hydrogen Energy 2018;43:9068–82.
[25] Ogawa Y, Hino M, Nakamura M, Matsunaga H. Pearlite-driven surface-cracking and associated loss of tensile ductility in plain-carbon steels under exposure to high-pressure gaseous hydrogen. Int J Hydrogen Energy 2021;46:6945–59. https://doi.org/10.1016/j.ijhydene.2020.11.137.
[26] Wang M, Akiyama E, Tsuzaki K. Effect of hydrogen and stress concentration on the notch tensile strength of AISI 4135 steel. Mater Sci Eng 2005;398:37–46. https://doi.org/10.1016/j.msea.2005.03.008.
[27] Wang M, Akiyama E, Tsuzaki K. Crosshead speed dependence of the notch tensile strength of a high strength steel in the presence of hydrogen. Scripta Mater 2005;53:713–8. https://doi.org/10.1016/j.scriptamat.2005.05.014.
[28] Wei Sun Y, Zhi Chen J, Liu J. Investigation into hydrogen diffusion and susceptibility of hydrogen embrittlement of high strength 0Cr16Ni5Mo steel. J Iron Steel Res Int 2015;22:961–8. https://doi.org/10.1016/S1006-706X(15)30097-2.
[29] Momotani Y, Shibata A, Terada D, Tsuji N. Effect of strain rate on hydrogen embrittlement in low-carbon martensitic steel. Int J Hydrogen Energy 2017;42:3371–9. https://doi.org/10.1016/j.ijhydene.2016.09.188.
[30] Álvarez G, Peral LB, Rodríguez C, García TE, Belzunce FJ. Hydrogen embrittlement of structural steels: effect of the displacement rate on the fracture toughness of high-pressure hydrogen pre-charged samples. Int J Hydrogen Energy 2019:44 15634–15643. https://doi.org/10.1016/j.ijhydene.2019.03.279.
[31] Barthelemy H. Effects of pressure and purity on the hydrogen embrittlement of steels. Int J Hydrogen Energy 2011;36:2750–8. https://doi.org/10.1016/j.ijhydene.2010.05.029.
[32] Ogawa Y, Matsunaga H, Yamabe J, Yoshikawa M, Matsuoka S. Unified evaluation of hydrogen-induced crack growth in fatigue tests and fracture toughness tests of a carbon steel. Int J Fatig 2017;103:223–33. https://doi.org/10.1016/j.ijfatigue.2017.06.006.
[33] Imdad A. Microstructure influence on hydrogen permeation and embrittlement of 4140 steel. Ph. D. Thesis, University of Oviedo; 2023.
[34] UNE-EN ISO 6892-1. Materiales metálicos. Ensayo de tracción. Parte 1: Método de ensayo a temperatura ambiente [n.d.]. 2016.
[35] Valentini R, Salina A. Influence of microstructure on hydrogen embrittlement behavior of 2.25Cr–1 Mo steel. Mater Sci Technol 1994;10:908–14. https://doi.org/10.1179/mst.1994.10.10.908.
[36] Parvathavarthini N, Saroja S, Dayal RK, Khatak HS. Studies on hydrogen permeability of 2.25% Cr-1% Mo ferritic steel: correlation with microstructure. J Nucl Mater 2001;288:187–96. https://doi.org/10.1016/S0022-3115(00)00706-6.
[37] Zakroczymski T, Szklarska-Śmiałowska Z, Smialowski M. Effect of arsenic on permeation of hydrogen through steel membranes polarized cathodically in aqueous solution. Mater Corros 1975;26:617–24. https://doi.org/10.1002/maco.19750260804.
[38] Arniella V, Zafra A, Alvarez G, Belzunce J, Rodríguez C. Comparative study of embrittlement of quenched and tempered steels in hydrogen environment. Int J Hydrogen Energy 2022;47:17056. https://doi.org/10.1016/j.ijhydene.2022.03.2. 1706.
[39] Yamabe J, Awane T, Matsuoka S. Investigation of hydrogen transport behavior of various low-alloy steels with high-pressure hydrogen gas. Int J Hydrogen Energy 2015;40:11075–86.
[40] del Busto S, Betegón C, Martínez-Pañeda E. A cohesive zone framework for environmentally assisted fatigue. Eng Fract Mech 2017;185:210–26. https://doi.org/10.1016/j.engfracmech.2017.05.021.